Chemical Engineering Journal 396 (2020) 125389

Contents lists available at ScienceDirect

Chemical Engineering Journal

journal homepage: www.elsevier.com/locate/cej

Anomalies detected during hydrodynamic cavitation when using salicylic acid dosimetry to measure radical production

Mojca Zupanc[a], Martin Petkovšek[a], Jure Zevnik[a], Gregor Kozmus[a], Alenka Šmid[b], Matevž Dular[a,*]

[a] Faculty of Mechanical Engineering, University of Ljubljana, Askerceva 6, 1000 Ljubljana, Slovenia
[b] Faculty of Pharmacy, University of Ljubljana, Askerceva 7, 1000 Ljubljana, Slovenia

HIGHLIGHTS

- High concentration of SA significantly influences cavitation dynamics.
- Physical and chemical explanations for the observed anomalies are given.
- Change in surface tension, coalescence and nucleation influence cavitation the most.
- Past results on radical formation by cavitation may be falsely interpreted.
- Special care needs to be given to cavitation characteristics in dosimetry studies.

GRAPHICAL ABSTRACT

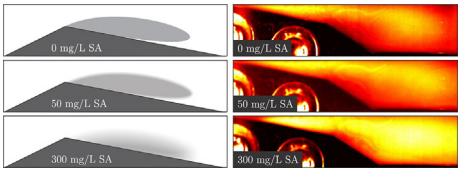

ARTICLE INFO

Keywords:
Cavitation
Salicylic acid dosimetry
Anomalies
Physical characteristics
Nucleation
Coalescence

ABSTRACT

Cavitation used to be associated with negative outcomes in hydraulic turbomachinery but nowadays it is often used for water cleaning, microorganism's destruction and degradation of organic compounds. This study investigated the amount of ·OH formed during hydrodynamic cavitation using salicylic acid dosimetry. The radical's amount was evaluated by quantifying the concentration of 2,3-dihydroxybenzoic acid, catechol and 2,5-dihydroxybenzoic acid. Two concentrations of the dosimeter in tap water were investigated, 50 and 300 mg L^{-1} (pH approx. 2.5). After 90 min of cavitation using a Venturi constriction a sum of the three products was determined at 0.97 μg mL^{-1} and 1.81 μg mL^{-1}, respectively. However, during the investigation the anomalies were detected in the cavitation development when higher concentration of salicylic acid was used – cavitation appeared more gentle, with less intense collapses, unrelated to the one in pure water. Detailed observations of cavitation and additional bubble dynamics simulations revealed that the decreased surface tension of the acidified salicylic acid solution is the most influential physical characteristic. Further experiments on nucleation and coalescence showed that high concentration of salicylic acid also leads to longer stability of the bubbles and prevents their coalescence due to short-range repulsive forces (steric hindrance), which results in less violent bubble collapse. We also discuss the importance of an appropriate amount of the dosimeter for correct evaluation of ·OH production in a given cavitation device (50 mg L^{-1} for the present one). This is essential for further cavitation exploitation studies to avoid false interpretation of the gathered results.

1. Introduction

Cavitation, nowadays a renowned topic among scientists, is a physical phenomenon accompanied by chemical processes that can occur in liquids. The phenomenon encompasses the growth and collapse of vaporous or gaseous cavities in a liquid as a consequence of the

* Corresponding author.
E-mail address: matevz.dular@fs.uni-lj.si (M. Dular).

https://doi.org/10.1016/j.cej.2020.125389
Received 31 January 2020; Received in revised form 6 May 2020; Accepted 6 May 2020
Available online 08 May 2020

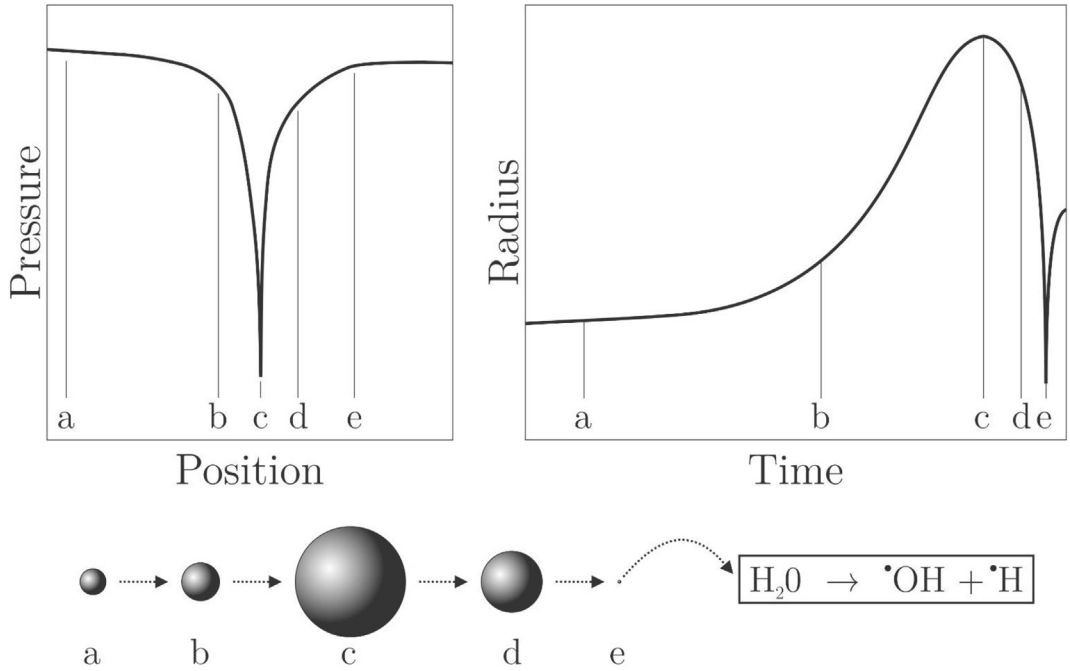

Fig. 1. In a typical Venturi section configuration, the pressure drops and then recuperates as the flow passes the throat (upper left diagram, a to e). This triggers the explosive growth of the cavitation nucleus and its subsequent collapse (upper right diagram and bottom sequence, a to e). At the moment of cavitation bubble collapse a local and instantaneous "hot spot" forms, what causes the dissociation of water molecules into ˙OH and ˙H.

local pressure drop and its recovery, respectively (Fig. 1). While the pivotal mechanism of bubble generation is in essence the same, the difference between the two most investigated cavitation types, acoustic (AC) and hydrodynamic cavitation (HC), is in the way the local pressure drops. In the case of HC, bubble inception can be for example triggered by acceleration of the liquid through a constriction such as Venturi section. With consecutive pressure recovery unstable cavities go through a violent spherical or asymmetrical collapse, releasing shock waves with a magnitude of up to 100 MPa [1] and high velocity microjets [2], respectively. In addition, short-term local hot spots can form at the centre of the bubble collapse with temperatures of presumably several 1000 K [3]. These extreme conditions result in above mentioned chemical process, namely homolysis of vaporous water molecules and formation of ˙OH and ˙H [4].

Even though cavitation has been in the centre of numerous investigations through the years there are many aspects of the phenomenon which still need to be elucidated. A big gap, for example, exists between observing and understanding the effects that addition of different compounds has on cavitation behaviour. Specifically, how it influences the governing mechanisms of cavitation, such as bubble growth and collapse. To get a better understanding of this aspect, basic experiments should thus be conducted in a simple matrix – tap water (TW) and then compared to behaviour in more complex matrices. With addition of different chemicals into the TW the characteristics of the final solution can change dramatically, and cavitation developed in these solutions could differ completely from the cavitation observed in TW. The most important physical characteristics of the solution that can thus influence cavitation are viscosity, vapor pressure, surface tension, the number of nuclei (presence of gas bubbles) and bubble coalescence. Besides the dynamics of a cavitating flow, these characteristics can also affect the behavior of single cavitation bubbles [5]. Vapor pressure therefore plays an important role in cavitation occurrence, since a higher vapor pressure of a fluid translates to a higher chance of cavitation development at given conditions. Similarly, nucleation can strongly affect the cavitation patterns and increase the likelihood of cavitation development [6]. Furthermore, viscous and surface tension effects grow with smaller spatial scales and can influence certain physical aspects of cavitating flow, such as supercavity detachment and cavitation inception. Additionally, viscosity tends to slow down explosion and collapse of bubbles. Although in case of water this effect is very weak, it can be important in other, strongly viscous liquids [7]. Surface tension, on the other hand, accelerates the collapse of bubbles and can also play an important role in their stability. Furthermore, number and size distribution of gas nuclei can be strongly affected by the rate of bubble coalescence. It is well known that surface-active additives play an important role in coalescence development, in general acting as its inhibitor [8]. They cause narrower bubble population distribution and a shift to smaller bubble radius [9]. There are two main mechanisms, which prevent coalescence occurrence: long-range electrostatic repulsive and short-range repulsive forces [10]. Ionic additives possess a formal charge, therefore when added to the solution their adsorption on the bubble-liquid interface charges the bubbles' surfaces. Bubbles are therefore repelled by a long-range electrostatic forces. These forces do not only prevent bubble coalescence but can also result in less dense bubble clusters [11]. On the other hand, non-ionic additives like aliphatic alcohols, prevent coalescence by short-range repulsive forces due to steric hindrance of their chains. In fact, the longer the alcohol's chain the greater the inhibition of coalescence [8]. By evaluating each of these characteristics, a better understanding of which one affects cavitation the most can be gained.

Evaluation of chemical processes can be performed with different dosimetry reactions, where compounds that can scavenge ˙OH are used. In this way the radicals are indirectly determined through the quantification of reaction products between the selected dosimeter and ˙OH [12]. Because of their electrophilic nature, ˙OH can attack electron rich sites of organic molecules [13]. This characteristic is exploited in dosimetry reactions where hydroxylation of aromatic compounds (i.e. salicylic acid, benzoic acid, p-chlorobenzoic acid) is exploited [14]. A few important criteria that every dosimeter should meet are i) a high reaction rate constant with ˙OH, ii) formation of stable products that can be easily quantified, iii) availability of a sensitive method for the determination of final products and iv) selectivity for ˙OH, meaning that the final products are formed exclusively by the reaction of ˙OH with the used dosimeter [15–17]. Because salicylic acid (SA) satisfies all

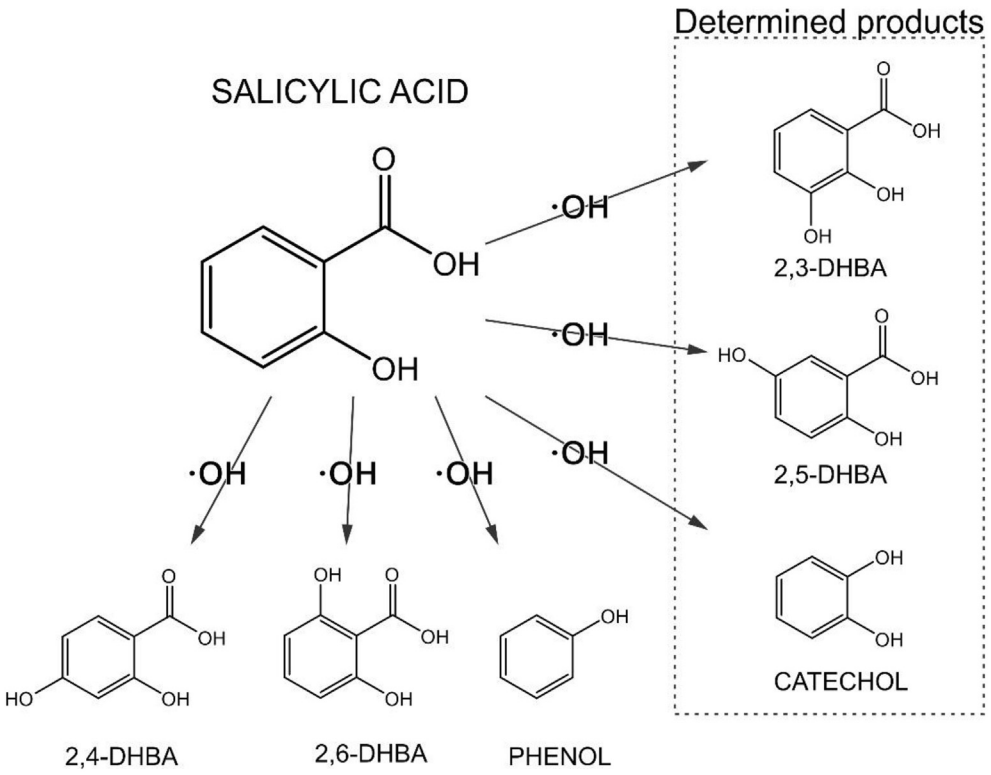

Fig. 2. Determined SA products after addition of ˙OH formed during cavitation on the aromatic ring (right) and possible products formed (bottom).

these criteria it is often used for evaluation of ˙OH production in a variety of advanced oxidation processes (AOP) (i.e. ozonation, heterogeneous photocatalysis, cavitation, Fenton chemistry, radiolytic oxidation, UV/H_2O_2) and biological processes [18].

Regardless of the AOP used, major products formed from the addition of ˙OH to SA are 2,3-dihydroxybenzoic acid (2,3-DHBA), 2,5-dihydroxybenzoic acid (2,5-DHBA) and catechol [16] (Fig. 2). The main difference between AOP's, is which end product is formed in majority [19] which depends on the presence of metals, catalysts and different gases [20]. Besides these three major products, also some other hydroxylated products like 2,4-DHBA and 2,6-DHBA can potentially form [21] together with products of aromatic ring breakage like 1,4-dihydroxybenzene, Z,Z-muconic acid, maleic acid, fumaric acid, D,L-malic acid, oxalic acid, malonic acid and acetic acid [18]. In one study also phenol was detected as one of the major SA products [22].

The first intent of this study was to investigate the influence of various cavitation conditions and types on ˙OH production using the SA dosimetry. To determine the formed SA products, a new analytical method using HPLC coupled to UV–Vis detector was developed. We focused on the formation of only the most probable monohydroxylation products.

Our investigation took a different direction when we noticed, by means of visualization and acoustic emission, that the cavitation changes once SA together with HCl was added to the TW sample. We consider this a major issue in the interpretation of the results of past studies which employed SA dosimetry in cavitation and possibly also in other AOP's. Thus, to determine which of the two added chemicals influences the detected anomalies the most, we performed a variety of experiments where we changed concentrations of SA and HCl. In this manner we have determined the concentration of both compounds at which the cavitation stays approximately the same as in TW and the formed SA products are still detected with HPLC.

In order to better understand what the reasons for the observed anomalies were, we additionally investigated the characteristics of a few chosen solutions in more detail (TW, TW with addition of HCl, TW with addition of SA and TW with addition of HCl with two different concentrations of SA). In addition to simultaneous high-speed visualization and pressure pulsation measurements, various physical characteristics (viscosity, vapor pressure, surface tension, nucleation and bubble coalescence) were determined. In addition to experimental investigations, we performed various numerical calculations based on Rayleigh-Plesset equation for a single cavitation bubble [5] to further substantiate our findings.

2. Materials and methods

2.1. Materials

High purity salicylic acid (SA) (≥99%), 2,3- dihydroxybenzoic acid (2,3-DHBA) (99%), 2,4-dihydroxybenzoic acid (2,4-DHBA) (97%), 2,5-dihydroxybenzoic acid (2,5-DHBA) (98%), 2,6-dihydroxybenzoic acid (2,6-DHBA) (98%), 3,4- dihydroxybenzoic acid (3,4-DHBA) (97%) and catechol (≥99%) were purchased from Sigma-Aldrich. 1 M HCl was purchased from Honeywell Fluka. Trifluoroacetic acid (99%, extra pure) was purchased by Acros Organics. Methanol (LiChrosolv®) for liquid chromatography was purchased by Merck. Stock solutions (20.0 mg mL^{-1}) of catechol, 2,3-DHBA, 2,4-DHBA, 2,5-DHBA and 2,6-DHBA were prepared in methanol. Working standard solutions were prepared on the day of analysis by dilution of the stock solutions with the chromatographic eluent (methanol-0.1% TFA solution) to give solutions in the concentration range of 0.016–4 μg mL^{-1}. Stock solutions were stored at −20 °C. Stock solution of SA was prepared in TW and was further diluted to prepare solutions with concentrations ranging from 50 to 300 mg L^{-1} on the day of experiments.

2.2. Cavitation test-rig

Experiments were performed in a small blow-through cavitation test-rig. Cavitation test section design (Fig. 3 left), firstly described in [23], is based on a symmetrical Venturi constriction, connected with

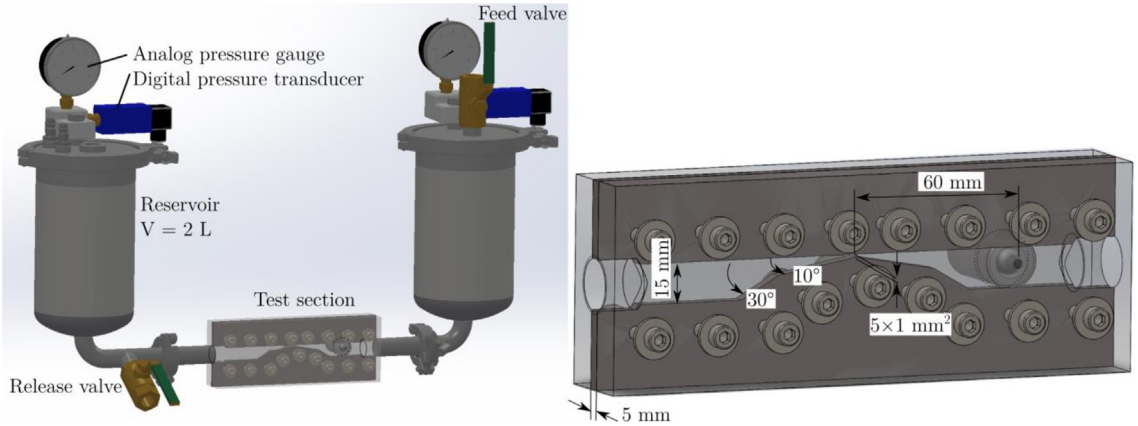

Fig. 3. Cavitation test-rig (left) and Venturi section (right). The flow is pushed from one reservoir to the other and then back through the Veturi section, where it cavitates.

two equal reservoirs (volume of 2 L each), and powered by a pressure difference between them. General working principle of the test-rig is to push the introduced sample from one reservoir into the other through the constriction, where cavitation forms by each pass. Using electrically controlled pneumatic valves, driven by Labview software, one can choose the number of passes at desired pressure difference. For the purpose of this investigation, the pressure difference of 7 bar was chosen, which corresponds to 5.5 s/pass for 1 L of sample.

Two angle convergent-divergent Venturi nozzle (Fig. 3 right) was designed in order to achieve more intensive pressure recuperation downstream the Venturi throat. This causes intense collapse of cavitation structures, resulting in high density energy release. The channel width and height equalled 5 mm and 15 mm respectively – the height was reduced to 1 mm at the throat. The entire test section (Fig. 3 right) was made of transparent acrylic glass in order to enable visualization of cavitation structures inside the Venturi constriction from various angles. In addition to high-speed visualization, the acrylic test section was designed so that pressure oscillations during experiments could be captured with high frequency pressure transducer.

2.3. Experimental procedure and equipment

For the determination of SA products, 1 L of SA solution was acidified with HCl prior to cavitation experiments. For the HPLC analysis 1 mL of the sample was taken after 0, 15, 30, 60 and 90 min of cavitation treatment. During the experiments the temperature of the samples increased, but it never exceeded 39 °C.

For the visualization, pressure pulsations, viscosity, surface tension, vapor pressure, nucleation and coalescence measurements, samples were prepared separately. Visualization and pressure pulsations were performed simultaneously using 1 L sample, while for the measurements of surface tension, viscosity, vapor pressure, nucleation and coalescence 150 mL, 100 mL, 400 mL, 1 mL and 150 mL samples were used, respectively.

High-speed visualization was performed using Photron FastCam SA-Z with possibility of 1-Megapixel at 20,000 fps and maximum frame rate of 2.100,000 fps. For the presented experiments the frame rate of 200,000 fps, at the resolution of 768 × 176 pixels was used. High power LED illumination allowed the setting of the shutter time down to 250 ns. To evaluate the aggressiveness of cavitation from the hydrodynamic point of view, pressure pulsations were measured with a PCB 113B28 high frequency pressure transducer, installed 60 mm downstream the constriction throat. The temperature was monitored using a resistance temperature sensor Pt100 (uncertainty of ± 0.2 K), installed directly into the reservoir of the cavitation test-rig. pH was measured using a Hach-Lange multimeter HQ430d and PHC725 probe. Viscosity was measured on an Anton Paar Physica MCR 301 rheometer equipped with a double gap measuring system DG26.7/T (concentric cylindrical system) as a function of a shear rate in the range of 0.1 to 100 s^{-1}.

Surface tension measurements were performed by Kruss tensiometer K12, using Wilhelmy plate method. Samples were mixed before the measurements and the temperature was held constant at 19 °C. A series of 6 or more measurements was performed for every investigated sample.

Vapour pressure was measured by lowering the pressure inside a closed glass bottle down to the boiling point using a vacuum pump. Thermocouple J-type (± 0.75%) and absolute pressure transducer ABB 266AST (± 0.04%) installed on the bottle cap were used to measure the temperature and pressure changes during the experiments, respectively. The measurements were performed continuously during a longer time period, where the starting temperature of the sample was cooled down from 38 °C to 28 °C. Pressure and temperature changes of the sample were simultaneously measured via NI cDaq 9219 measurement card.

Nucleation was determined by high-speed visualization of micro bubbles, induced by intense sample shaking. For this purpose, a vertical shaking mechanism was designed. Firstly, 1 mL of the sample was pipetted into a 3 mL semi-micro cuvette, made of acrylic glass. The cuvette was then attached to the shaker and shaken vertically with 45 Hz and 2 cm amplitude. The shaking stopped after 60 periods and then the camera was triggered. Fastec HiSpec4 camera at 300 fps, equipped with Nikon 105 mm macro lens and 68 mm extension tube was used. Diffuse backlight illumination was achieved by Vega Velum optical fibre light source. Captured photos were then pre-processed and the circular Hough transform algorithm with high sensitivity parameters was used to detect multiple overlapping bubbles. Afterwards several filters were applied to eliminate false detections.

Adjacent capillaries experiment was performed to examine potential coalescence inhibition of additives. Two polytetrafluoroethylene (PTFE) capillaries of 2 mm inner and 4 mm outer diameter respectively, were submerged into the examined solution. Air was being blown through each capillary using a syringe until a stable bubble was formed on the capillary tip. The capillaries were then aligned horizontally and slowly moved closer to each other using micrometric positioning system. Photron Fastcam Mini UX100 high-speed camera together with Nikon 105 mm macro lens and Vega Velum optical fibre backlight illumination was used to observe the procedure. The distance between capillaries at the moment of coalescence was then measured from images. In order to determine which repulsive forces, the long-range electrostatic or the short-range ones, are responsible for coalescence inhibition, we added appropriate amount of NaCl to form a 0,1 M NaCl solution and repeated the experiment.

All the experiments performed during this study were made in TW and are presented in Table 1. Experiments were performed in multiple

Table 1
Experiments performed during this study.

pH SA [mg L^{-1}]	-	4.5	4	3	2.5
0	A, B, C, E, F, G, H	/	A, B	/	A, B, C, E, H
50	A, B	A, B, D	A, B, D	A, B, D	A, B, C, D, E, H
100	A, B	A, B	A, B	A, B	A, B
150	A, B	A, B	A, B	A, B	A, B
300	A, B, C, E, H	/	A, B	/	A, B, C, D, E, F, G, H

A: pressure pulsations; B: high-speed camera visualization; C: surface tension; D: SA products; E: nucleation; F: viscosity; G: vapor pressure; H: coalescence; -: no addition of HCl; /: no experiments were performed

parallels. Deviations between parallel experiments in the case of SA products determination were below 20% except in the case of catechol (standard deviation of 52%, 15 min), due to small concentrations. Pressure pulsations were captured in three series, each 1 s long. Each series was taken during a new pass through the Venturi constriction in order to determine deviation between the measurements (below 30%). The values obtained between the series in vapor pressure measurements did not exceed 2% of the measured value.

2.4. Chromatographic conditions for SA products analysis

The analyses were performed on high performance liquid chromatography system (HPLC Agilent Infinity 1260), equipped with a quaternary pump, a degasser, an autosampler, an injector with a 100 µL sample loop, a column oven, and diode array detector. Data were recorded and evaluated using Agilent OpenLAB software. Separation of compounds was performed on a 4 mm × 125 mm, 5 µm particle size, LiChrospher® 60 RP-Select B column (MZ-Analysentechnik GmbH, Germany) using isocratic elution with a mobile phase consisting of methanol and 0.1% trifluoroacetic acid (pH = 2.0) (20 : 80, v/v). The mobile phase flow rate was 1.0 mL min^{-1}, which resulted in the retention times of about 3.2 min for catechol, 5.2 min for 2,6-DHBA, 6.1 min for 2,5-DHBA, 8.5 min for 2,3-DHBA and 9.4 min for 2,4-DHBA. The peak areas were monitored by a diode-array detector at four wavelengths (247 nm, 258 nm, 278 nm and 320 nm). The injection volume was 100 µL for all sample solutions.

3. Results

3.1. Analytical method validation

Linearity was established by least-squares linear regression analysis of the calibration curve. The constructed calibration curves were linear over the concentration range of 0.03–2.0 µg mL^{-1}. For all the compounds, the correlation coefficient values (0.9997–0.9999) show that the methods were linear in the specified range. In order to determine repeatability, six parallels of samples containing known amount of standards at three different concentrations (1 µg mL^{-1}; 0.5 µg mL^{-1}; and 0.05 µg $mL^{-}1$) were prepared and analysed. The calculated relative standard deviation (RSD %) ranged from 0.1 to 2.5%. The regression equations, correlation coefficients, RSD and LOD values are summarized in Table 2.

Representative chromatograms of standard containing all analytes are presented in Fig. 4. Quantification of analytes was performed at different wavelengths: catechol at 278 nm, 2,3-DHBA and 2,6-DHBA at 247 nm, 2,4-DHBA at 258 nm and 2,5-DHBA at 320 nm.

3.2. Salicylic acid dosimetry

In the existing literature where SA dosimetry was used for the determination of ˙OH during cavitation, the initial concentrations of SA ranged from 50 to 1500 mg L^{-1} [15,19,21,12,20,18]. Based on this, an initial concentration of 300 mg L^{-1} of SA was selected for the experiments performed in this study. Since in cavitation ˙OH form inside the cavitation bubbles and can only reach the gas-liquid interface, the dosimeter must reach these radical rich sites [12]. SA seems a perfect dosimeter since we can easily manipulate its characteristics by changing the pH [12]. For this purpose, the samples were acidified to below the pKa of SA (pKa = 2.97), where its molecular form predominates thus assuring its hydrophobicity and presence in the gas-bubble interface [19,12].

It can be observed from the results presented in Fig. 5 that the concentration of the formed SA products was increasing with time linearly up until 60 min. After 90 min only a small increase in the concentration could be observed. The reasons for this are at the moment not completely understood and will be the focus of our future study. Under the presented experimental conditions only three hydroxylated SA products were detected, which is in accordance with the literature. The 2,3-DHBA was formed in majority followed by catechol and 2,5-DHBA. The reason why 2,3-DHBA is the preferred product probably lies in the fact that –COOH and –OH groups of the SA molecule direct the site of ˙OH attack, making ortho and para positions relative to –OH, the ones with the highest electron density and thus primarily subjected to the attack of the electrophilic ˙OH [24,13].

It is hard to compare our results in more detail with the available literature (i.e. the concentration of formed products), since the experiments in the literature were performed in deionised water and mostly using AC and not HC. It is important to be aware that based on the water matrix used, different cavitation conditions can ensue, which can all affect formation of SA products. Comparison between AC and HC is additionally difficult due to different energy input of the two processes. Nevertheless, our results are in accordance with Chakinala

Table 2
Main validation parameters determined for the HPLC analysis.

Analyte	Linearity range (µg mL^{-1})	Regression equation	Correlation coefficient (r^2)	RSD (%) (n = 6)			LOD (µg mL^{-1})
				A	B	C	
Catechol	0.03 – 2.0	y = 609.8*x + 12.42	0.9999	0.1	0.2	2.3	0.01
2,3-DHBA	0.03 – 2.0	y = 1410*x − 37.19	0.9997	0.3	0.2	0.7	0.02
2,4-DHBA	0.03 – 2.0	y = 2558*x − 9.443	0.9999	0.2	0.4	0.4	0.02
2,5-DHBA	0.03 – 2.0	y = 671.5*x − 7.615	0.9998	0.3	0.4	2.5	0.02
2,6-DHBA	0.03 – 2.0	y = 1122*x − 15.04	0.9999	0.2	0.2	1.3	0.02

A: tested at the expected high concentration (1 µg mL^{-1}); B: tested at the middle concentration (0.5 µg mL^{-1}); C: tested at the low concentration (0.05 µg mL^{-1}).

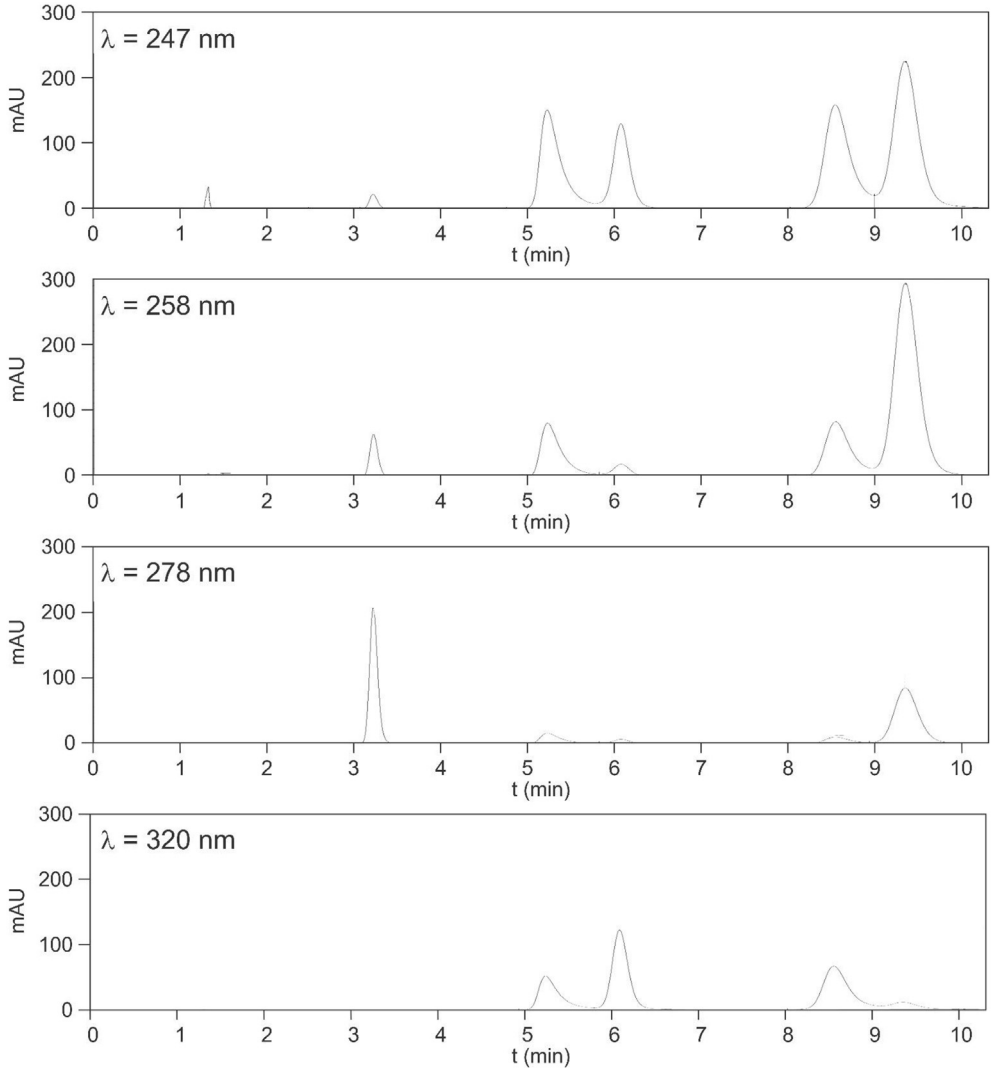

Fig. 4. Chromatogram of a standard solution containing 2 μg mL^{-1} of catechol (Tr = 3.2 min), 2,6-DHBA (Tr = 5.2 min), 2,5-DHBA (Tr = 6.1 min), 2,3-DHBA (Tr = 8.5 min) and 2,4-DHBA (Tr = 9.3 min).

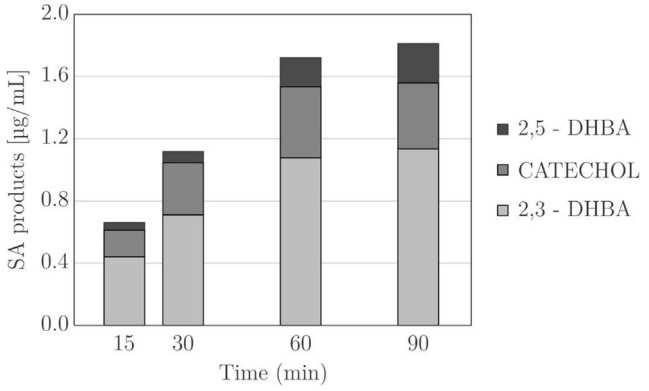

Fig. 5. Concentrations [μg mL^{-1}] of the three major SA products determined during a 90 min cavitation experiment at initial concentration of 300 mg L^{-1} SA in TW, 7 bar pressure difference and pH = 2.65. The results show that the concentration of formed products is increasing linearly with time up until 60 min but then the rate of product formation decreases. The main product formed from the interaction of ˙OH with SA was 2,3-DHBA followed by catechol and 2,5-DHBA.

and co-workers [20] and Martínez-Tarifa and co-workers [21], who also determined 2,3-DHBA as the preferred product using AC. Additionally, Martínez-Tarifa and co-workers [21] developed a HPLC method for determination of 2,4-DHBA and 2,6-DHBA but did not detect them, which is also in accordance with our results. On the other hand, Arrojo and co-workers [19] and Amin and co-workers [15] reported that during HC experiments no catechol formed. Additionally, Arrojo and co-workers [19] reported that 2,5-DHBA was the preferred SA product, which is contradictory to our results. This inconsistency could be the result of different HC set-ups used. Arrojo and co-workers [19] used a pump + constriction device where cavitation appears in the constriction but can in addition also develop in the pump impeller, which could result in different cavitation conditions and thus influence the discrepancy in the results [25].

We must be aware that these results represent only a conservative estimation of ˙OH formed during cavitation. Even though we can manipulate the chemical characteristics of the dosimeter so it is found in the gas-liquid interface, we still cannot prevent the recombination of ˙OH inside the gas phase. Besides this, some other compounds could potentially form which were not in the scope of this investigation and were thus not taken into account like: i) polyhydroxylated products which can form by addition of more than one ˙OH to the aromatic ring of SA, ii) products formed as a result of the aromatic ring cleavage of SA

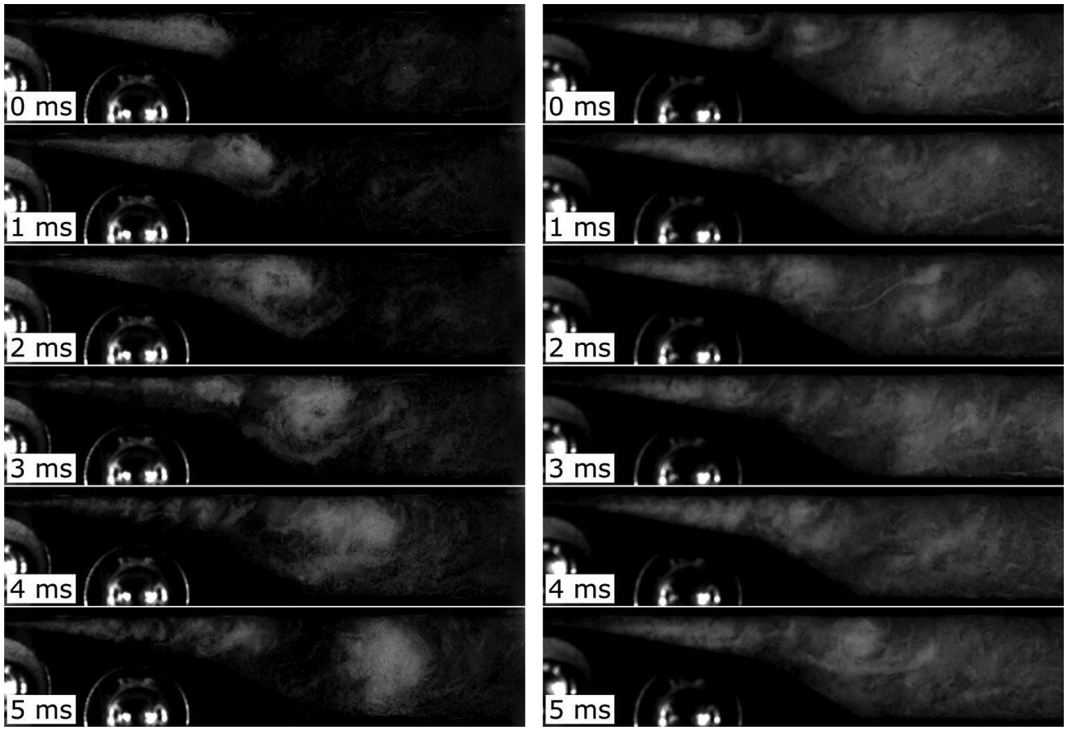

Fig. 6. Typical cavitating flow in a Venturi section observed in TW (left) and a solution of 300 mg L^{-1} SA, pH = 2.65 (right). Cavitation in TW forms strong cloud shedding, while cavitation in a solution of 300 mg L^{-1} SA results in stable conditions with weak dynamic activities. In the solution of 300 mg L^{-} SA formed cavitation bubbles stay present in the flow for much longer than in TW.

or its products (i.e. short carboxylic acids, aldehydes, ketones and mineralization products – CO_2 [26]) or iii) H_2O_2 formed due to the ˙OH recombination. If one wanted to determine the exact amount of radicals formed during cavitation, all these different species should be monitored. In addition, dissolved inorganic solutes present in TW such as HCO^{3-}, $CO_3{}^{2-}$, $NO_2{}^{-}$, Br^{-}, and I^{-} can also act as ˙OH scavengers [27].

Recombination of ˙OH that reach the gas-liquid might be minimized if the amount of the dosimeter is augmented in this area [19] but based on the anomalies detected during this study this might not be the best solution in the case of HC. During our experiments with high-speed camera we observed that cavitation structures, when SA was added in the concentration 300 mg L^{-1}, were completely different compared to TW. The observed anomalies are in more detail described below.

3.3. Cavitation issue

Cavitation appearance in TW and a solution of 300 mg L^{-1} SA with addition of HCl (pH = 2.65) is presented in Fig. 6. Initial cavitation conditions (i.e. sample volume and pressure difference between the reservoirs) were the same in both cases. Flow conditions in TW formed developed cavitation with strong cloud shedding, while cavitation in TW + 300 mg L^{-1} SA + HCl (pH = 2.65) solution resulted in weak dynamic activities with formation of stable bubbles along the whole divergent part of the Venturi section. The difference between these two samples was detected not only by means of visualizations but also by means of acoustic emission. While cavitation in TW seems to be aggressive, pulsating and noisy, cavitation in TW + 300 mg L^{-1} SA + HCl (pH = 2.65) solution appears to be soft and gentle. In addition to high-speed visualization also pressure fluctuations (Fig. 7) show that cavitation in TW + 300 mg L^{-1} SA + HCl (pH = 2.65) behaves differently than cavitation in TW. Visualizations of cavitation appearance in various solutions are presented in Fig. 7, where comparison between cavitation in TW, TW + addition of HCl (pH = 2.48), TW + addition of 300 mgL^{-1} SA, TW + 300 mg L^{-1} SA + HCl (pH = 2.65) and TW + 50 mg L^{-1} SA + HCl (pH = 2.54) is shown. The average cavitation extent presents the average calculated image for time lap of 0.1 s. It presents an average size of cavitation developed inside the Venturi constriction or average cavitation probability. The colorbar qualitatively presents the density of cavitation bubbles in certain area, where black means no bubbles (solid wall, defining the geometry of Venturi constriction) and white means the maximum brightness of all presented cases. The brightness of images can be roughly connected with the void fraction ratio, where brighter sections of images mean higher fraction of vapour phase within the liquid. Standard deviation of visualization is calculated for the same visualization images. It gives the information on how the intensity of the brightness of images changes in the analysed period of time. This can be directly correlated to the intensity of the cavitation dynamics in the Venturi constriction, where brighter colour means more intense cavitation dynamics.

Comparing all these five cases, one can notice a distinctive difference between TW + 300 mg L^{-1} SA + HCl and all the other solutions. In the case of TW + 300 mg L^{-1} SA + HCl the cavitation bubbles fill the whole divergent part of the Venturi section and have a much lower tendency of collapsing. This can be seen in the average cavitation extent as a large bright area (large averaged cavitation extent) and in the intensity of cavitation dynamics as a dark area (low cavitation dynamics).

In the scope of the study we gradually decreased the amount of SA from 300 mg L^{-1}, 150 mg L^{-1}, 100 mg L^{-1} to 50 mg L^{-1} (Table 1) in order to determine the SA concentration where OH radicals can still be detected without influencing cavitation dynamics. In addition to various amounts of SA also different pH (2.5, 3, 4, 4.5) were tested to compare cavitation dynamics. For all amounts of SA and various pH conditions high-speed visualization and pressure pulsations were measured and compared. With reduction of SA concentration, also cavitation dynamics gradually resembles the one in pure TW. The presented results show that when 50 mg L^{-1} of SA was used (TW + 50 mg L^{-1} SA + HCl), cavitation resembled the one generated in TW. In the manuscript only results at extreme SA and HCl concentrations (300 and

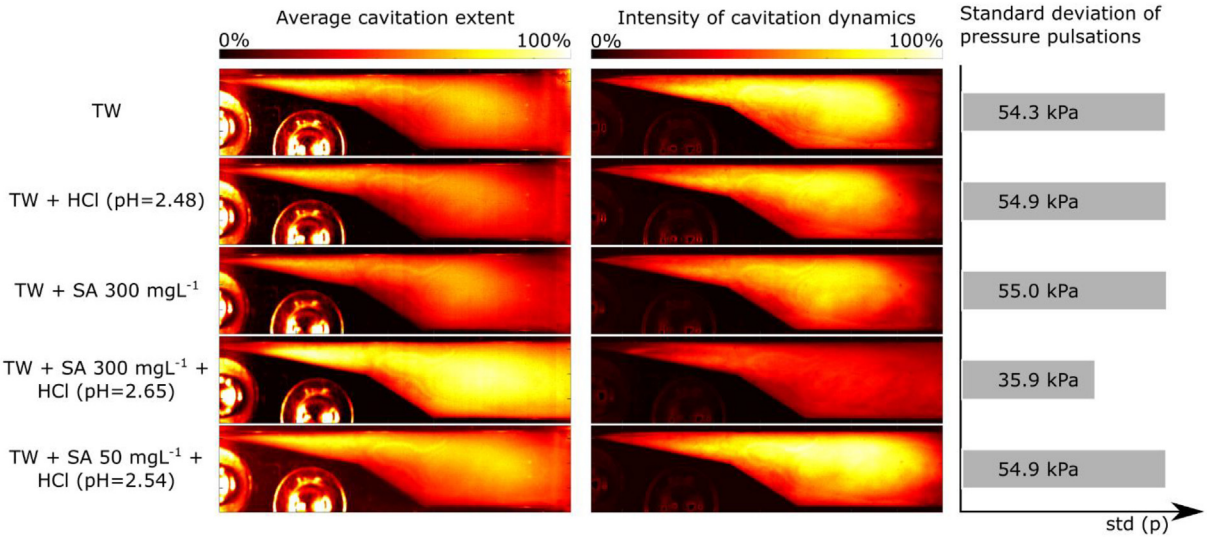

Fig. 7. Statistical analysis of cavitation appearance and dynamics in different solutions. Cavitation characteristics (left – average cavitation extent, middle – intensity of cavitation dynamics, right – standard deviation of pressure pulsations) for various investigated samples. Cavitation in a solution of 300 mg L^{-1} SA (pH = 2.65) is clearly standing out in comparison to cavitation in TW and other investigated solutions in terms of cavitation extent, dynamics and pressure pulsations. Cavitation in a solution of 50 mg L^{-1} SA (pH = 2.54) resembles cavitation in TW more than the one with 300 mg L^{-1} SA (pH = 2.65).

50 mg L^{-1} SA, pH = 2.5) are shown and possible explanations for synergistic effects of SA and HCl addition on cavitation dynamics are discussed in chapter 4. Discussion.

3.4. Salicylic acid concentration issue

Based on the results presented above we selected the concentration of 50 mg L^{-1} of SA for further experiments. To determine the optimal pH at which the highest amount of SA products is formed 4 different pH (4.5, 4, 3 and 2.5) were investigated. SA products were detected only at pH of 3 and 2.5 (Fig. 8). Our results are in agreement with Arrojo and co-workers [19], where the highest amount of SA products was detected at pH $<$ 3. Similar to the case with 300 mg L^{-1} the 2,3-DHBA product formed in the highest amount, followed by catechol and 2,5-DHBA. By far the highest sum of all SA products was determined after 90 min of cavitation. The higher results observed in the case of 30 and 60 min at pH = 3 are inside the measurement error.

When we compare the sum of concentrations of SA products formed with 300 mg L^{-1} of added SA (c = 1.81 μg mL^{-1}) to the results where 50 mg L^{-1} of SA was added to TW (c = 0.97 μg mL^{-1}), we see that the amount of SA products is higher with higher SA concentration, even though SA was in excess in both cases. This could be because there was

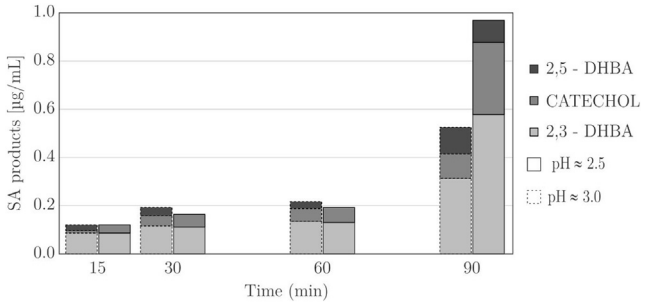

Fig. 8. Concentrations [μg mL^{-1}] of the three major SA products determined during 90 min cavitation experiment at initial concentration of 50 mg L^{-1} SA in TW, 7 bar pressure difference and two different pH = 2.5 and pH = 3.04. The results show that the highest concentration of formed products was determined at pH = 2.5 after 90 min of cavitation. The main product formed from the interaction of ˙OH with SA was once again 2,3-DHBA followed by catechol and 2,5-DHBA.

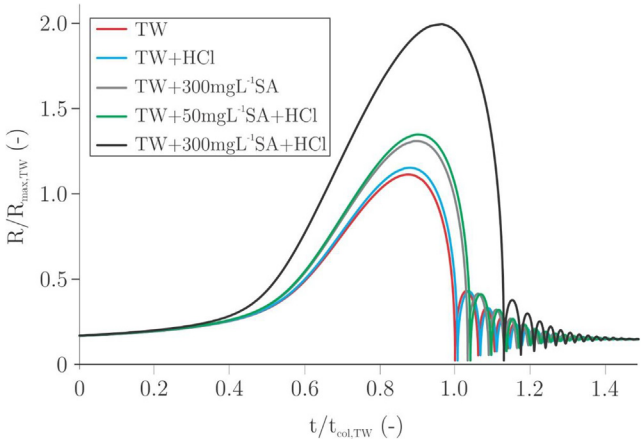

Fig. 9. The dynamics of an initially stable bubble nucleus after it is exposed to an oscillating pressure field. The dynamics clearly shows that the slight change in surface tension of the solution results in a significant response of the nucleus to the pressure change.

more SA available when higher concentration was used, and it is more probable that a SA molecule encounters a radical. However, we must be aware that the amount of the formed SA products was not proportionally higher when higher concentration of SA was added. This leads to a different conclusion which is that higher concentration of added SA negatively affects the formation of radicals. Higher concentration of SA together with higher amount of formed SA products leads to their augmented concentration at the gas-liquid interface which could lead to their higher evaporation into the cavitation bubble. The presence and degradation of these compounds inside the bubble could affect the bubble collapse temperature. The consequence of anomalies we detected during experiments described in this study, is less intense cavitation which affects the water molecule homolysis and radical formation. Singla and co-workers [22] noticed the same trend with benzoic acid. They postulated that with an increase of benzoic acid concentration the amount of generated ˙OH decreases. They attributed the reason for this to the pyrolytic decomposition of benzoic acid inside the cavitation bubble which decreases the release of heat at bubble collapse which corresponds to lower temperature and thus the lower amount of ˙OH formed. When the amount of the investigated substance

is increased its concentration on the gas-liquid interface of the cavitation bubble increases, which facilitates its evaporation into the bubble. These molecules in the gas phase of the bubble consume part of the heat energy that is produced when the bubble collapses [22]. Together with this the hydrocarbon products formed with the pyrolysis of the evaporated substance also decrease the bubble collapse temperature which additionally leads to a lower amount of formed ˙OH [22]. Similar disproportionality of results was also observed by Braeutigam who investigated the effect of different AC parameters on formation of ˙OH [28].

4. Discussion

Cavitation development, the amount and size of the bubbles and the intensity of their collapse depends on many physical characteristics of the liquid, namely viscosity, vapor pressure, surface tension and bubbles' ability to coalesce. Increased viscosity of the investigated liquid can for example influence the growth and collapse of the bubbles and thus result in changed cavitation intensity [5]. Vapor pressure of the solution influences the vapour to gas ratio inside the cavitation bubble and therefore its collapse intensity and consequently cavitation behaviour [1]. The presence of different chemicals in the sample can decrease surface tension [29]. Currell and co-workers [30] suggested that when the surface tension is lowered, more bubbles form under cavitating conditions due to these changed characteristics of the solution. Adding surface-active additives to the water matrix can greatly inhibit bubble coalescence. Several researchers have investigated their effect on acoustic cavitation. Coalescence prevention in general enhances cavitation in terms of sonoluminescence intensity [31] and even changes its spatial distribution [32]. However, surfactant effect on hydrodynamic cavitation has not been yet examined in detail.

In order to determine which of these physical characteristics was responsible for the observed anomalies in our study, we performed several experiments (Table 1). Our results showed that the addition of SA and HCl did not alter viscosity and vapor pressure of the solutions. Thus, the observed changes of cavitation development (Figs. 6 and 7) cannot be attributed to these two characteristics. However, surface tension of the investigated solutions did vary (Table 3), which points to the fact that this parameter is critical in the case of the observed cavitation anomalies. As shown in Table 3, the addition of chemicals into TW decreases surface tension. It can be seen that SA influences this parameter more than addition of HCl. Besides that, also the concentration at which SA is added plays an important role. When SA was added in 300 mg L^{-1} and acidified, the surface tension differed the most from the one determined in TW (58.67 mN m^{-1} compared to 72.96 mN m^{-1}, respectively).

The effect of surface tension change can be easily depicted by solving the Rayleigh-Plesset equation for bubble dynamics [5]. By choosing an initially stable cavitation nucleus and exposing it to an oscillating pressure field one can observe its response.

The only parameter, which was altered in the 5 simulations is the surface tension (according to the values given in Table 3). One can see that it plays a dominant role in the dynamics of bubbles. As in the above described experiment (Fig. 7), it can be seen that the case of TW + 300 mg L^{-1} SA + HCl deviates significantly from the others.

Additional experiments on nucleation by shaking the solutions and observing the stability of bubbles were performed. The process was observed by a high-speed camera and the number and sizes of the bubbles were determined, from these the instantaneous void fraction was calculated. Fig. 10 shows the trends together with the instantaneous images of the region of interest (6 by 6 mm in size) taken 500 ms after the end of shaking.

Table 3
Measurements of surface tension in different TW solutions at 19 °C.

Sample	σ [mN/m]
TW	72.96 ± 0.03
TW + HCl (pH = 2.48)	72.52 ± 0.02
TW + 300 mg L^{-1} SA	69.19 ± 1.27
TW + 300 mg L^{-1} SA + HCl (pH = 2.65)	58.67 ± 2.3
TW + 50 mg L^{-1} SA + HCl (pH = 2.54)	66.94 ± 3.5

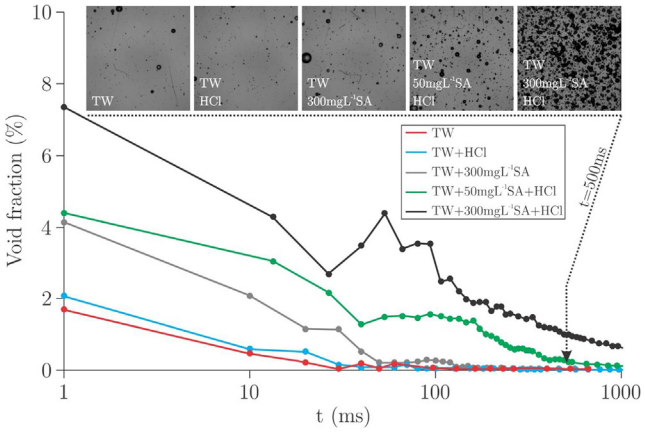

Fig. 10. Time evolution of the void fraction for the 5 specimens after the shaking test. One can see that all follow an exponentially decreasing trend, but only in the case of specimen with TW + 300 mg L^{-1} SA + HCl the bubbles remain large after a significant period of time.

The diagram is in a logarithmic scale, hence an exponentially decreasing void fraction can be observed for all specimens. The buoyancy plays an insignificant role during the one second of observations as the process is highly inertially driven. This is also the reason that the void fraction occasionally rises (for example in the case of TW + 300 mg L^{-1} SA + HCl at approximately 60 ms), when more bubbles are moved by the flow into the measuring region of interest.

One can notice that in specimens with TW, TW + HCl and TW + 300 mg L^{-1} SA the bubbles dissolve rapidly. The specimen with TW + 50 mg L^{-1} SA + HCl follows this dynamics relatively closely. The case is different for TW + 300 mg L^{-1} SA + HCl where the bubbles remain stable for a prolonged period of time, which is long enough for the nuclei to "live" until the next passage through the Venturi constriction where they significantly influenced the initial and consequent bubble dynamics.

This stabilization of bubbles could be due to the effect added chemicals have on bubble rate of coalescence. Coalescence inhibition was examined by performing an adjacent capillaries experiment. Two capillaries, submerged into the solution with air bubbles on their tips, were slowly moved closer to each other until coalescence happened (Fig. 11 – left). Fig. 11 – right shows average distances between capillaries at the moment of coalescence for different water solutions, containing HCl, SA and a combination of both. It can be seen there is almost no difference between TW (red), TW + HCl (blue) and TW + 300 mg L^{-1} SA (grey) solution. However, there is noticeable distance drop when HCl and SA are combined (green and black), suggesting there is a significant coalescence inhibition. The results are expected since when HCl and SA are combined, SA is in a protonated state and highly hydrophobic (discussed in detail in chapter 3.2 Salicylic acid dosimetry). Therefore, it is in majority located at the bubble–liquid interface and can influence bubble interactions. When the concentration of SA is higher, the coalescence inhibition is slightly more pronounced as there are probably more molecules of SA located on the bubble surface. However, when there is no HCl present in SA solution, SA is deprotonated and does not act as a surface-active molecule. Additionally, HCl alone does not affect coalescence as was demonstrated by Henry and co-workers [33].

To further examine which mechanism of coalescence inhibition governs the anomalies detected using SA, we added NaCl (to form a 0,1

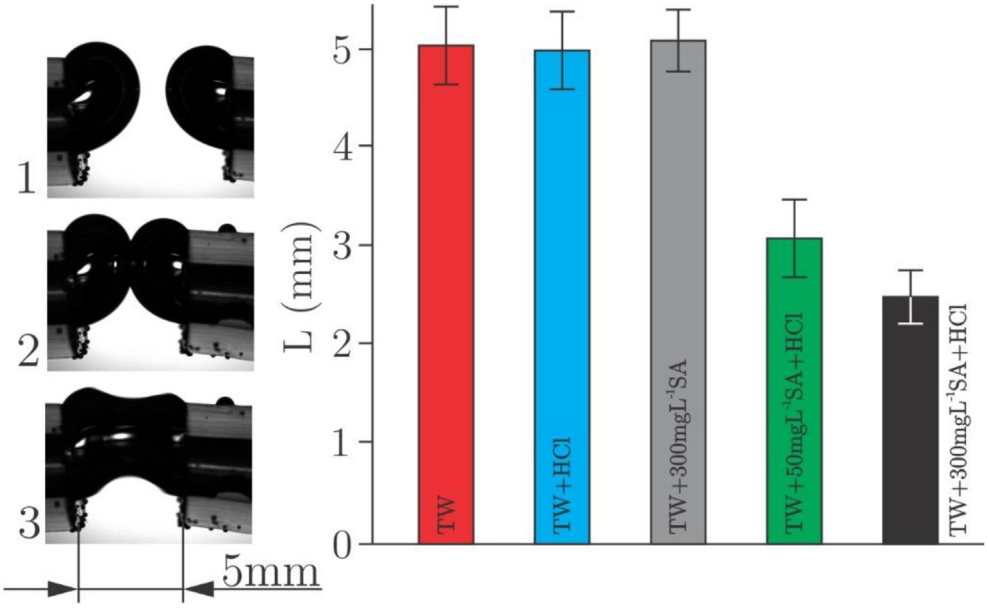

Fig. 11. Left: frame sequence of experiment for TW + 300mg L^{-1} SA solution: 1) onset, 2) one frame before coalescence, 3) coalescence. Right: the average distances between capillaries at the moment of coalescence for examined solutions.

M NaCl solution) to specimens containing both HCl and SA. Addition of an electrolyte like NaCl screens electric field between bubbles and decreases long-range electrostatic repulsive forces [11], thus eliminating this type of coalescence inhibitory effect. Since we have not noticed any difference between solutions with and without NaCl we can conclude that long-range electrostatic repulsive forces are not responsible for the bubble coalescence inhibition in our case. This result is in accordance with previous discussion (chapter 3.2 Salicylic acid dosimetry). Since SA is in a protonated state it does not possess a formal charge, so there are no electrostatic forces to screen. Zahradnik and co-workers have for example demonstrated that coalescence inhibition is more pronounced when alcohols' chains are longer, due to greater steric hindrance [8]. We can presume that a benzene ring causes similar steric hindrance as aliphatic chains of alcohols. We can thus conclude that SA coalescence inhibitory effect is mainly due to short-range repulsive forces caused by steric hindrace of SA molecule.

All performed experiments have shown that HCl and SA alone have little to no effect on solution's physical characteristics. However, when HCl and SA are combined, solution's surface tension and bubbles' ability to coalesce are significantly lowered. As a consequence, cavitation nuclei population is increased (Fig. 10), what, together with the sole effect of surface tension (Fig. 9), eventually leads to completely different cavitation dynamics (Fig. 7).

5. Conclusions

This study investigated ·OH formation and the anomalies detected during hydrodynamic cavitation when salicylic acid dosimetry was used (addition of SA and HCl). Experiments were performed in a blow-through cavitation test-rig with Venturi constriction. For this purpose also a novel analytical method was developed and used to determine and quantify three major SA products: 2,3- DHBA, catechol and 2,5-DHBA. Two different concentrations of SA in acidified TW were tested: 300 and 50 mg L^{-1} (pH approximately 2.5). The results showed that in both cases the major SA product formed was 2,3-DHBA followed by catechol and 2,5-DHBA. More SA products formed when higher SA concentration was used (1.81 μg mL^{-1}) as compared to lower SA concentration (0.97 μg mL^{-1}) but the augmentation was not proportionate. We thus concluded that high amount of SA negatively affects the amount of formed radicals and that lower concentration is more appropriate for accurate determination of OH radicals.

Anomalies at cavitation formation during the experiments performed with 300 mg L^{-1} SA (acidified TW, pH = 2.65) were captured by high-speed visualization and measurements of pressure pulsations. The results were compared to experiments performed in pure TW, acidified TW (pH = 2.48), 300 mg L^{-1} SA in TW and 50 mg L^{-1} SA in acidified TW (pH = 2.54). Stronger cavitation extent, smaller intensity of cavitation dynamics and significantly smaller deviation of pressure pulsations were determined in the first case (300 mg L^{-1} SA, pH = 2.65). To determine what causes these anomalies we additionally determined viscosity, vapor pressure, and surface tension of the investigated solutions. Our results showed that only surface tension plays an important role and lower value was determined in the case of acidified solution of 300 mg L^{-1} SA ($\sigma = 58.67 \pm 2.3$ mN m^{-1}) as compared to pure TW ($\sigma = 72.96 \pm 0.03$ mN m^{-1}). The results were further corroborated by Rayleigh-Plesset equation for bubble dynamics and by performing nucleation and coalescence experiments of the investigated solutions, which are in close relation with surface tension. Results showed that bubbles in acidified solution with higher concentration of SA remain stable longer, which is in accordance with what was observed during visualization. The coalescence experiments showed that short-range repulsive forces (consequence of steric hindrance) are responsible for coalescence inhibition. In the end we have shown that cavitation resembles the conditions formed in TW when 50 mg L^{-1} of SA in acidified solution is used.

When trying to capture as many radicals as possible and minimize their recombination during cavitation one can always increase the amount of added scavenger. However, the presented results show sensitivity of the cavitation process to the properties of the liquids, and obviously point to the fact that special care needs to be taken, when evaluating the production of radicals in such flows, and possibly in other AOPs, also.

Declaration of Competing Interest

The authors declare that they have no known competing financial interests or personal relationships that could have appeared to influence the work reported in this paper.

Acknowledgements

The authors acknowledge the financial support from the European Research Council (ERC) under the European Union's Framework Program for research and innovation, Horizon 2020 (grant agreement n° 771567 — CABUM) and the Slovenian Research Agency (research core funding No. P2-0401, P1-0208 and J7-1814).

We thank prof. dr. Odon Planinšek from the Faculty of Pharmacy (University of Ljubljana) for providing the equipment for the surface tension experiments. We additionally thank prof. dr. Aleš Ručigaj (University of Ljubljana) from Faculty of Chemistry and Chemical Technology for providing the equipment for viscosity measurements.

References

[1] C.E. Brennen, Cavitation and Bubble Dynamics, Oxford University Press, Pasadena, California, 1995.
[2] G.L. Chahine, C.-T. Hsiao, Modelling cavitation erosion using fluid-material interaction simulations, Interface Focus. 5 (2015) 20150016. doi: 10.1098/rsfs.2015.0016.
[3] K.S. Suslick, N.C. Eddingsaas, D.J. Flannigan, S.D. Hopkins, H. Xu, Extreme conditions during multibubble cavitation: sonoluminescence as a spectroscopic probe, Ultrason. Sonochem. 18 (2011) 842–846, https://doi.org/10.1016/j.ultsonch.2010.12.012.
[4] Y. Benito, S. Arrojo, G. Hauke, P. Vidal, Hydrodynamic cavitation as a low-cost AOP for wastewater treatment : preliminary results and a new design approach, WIT Trans. Ecol. Environ. 80 (2005) 495–503.
[5] J.P. Franc, J.M. Michel, eds., Fundamentals of cavitation, Kluwer Academic Publishers, USA, 2004. doi: 10.1017/CBO9781107415324.004.
[6] L. Briançon-Marjollet, J.P. Franc, Transient bubbles interacting with an attached cavity and the boundary layer, J. Fluid Mech. 218 (1990) 355–376, https://doi.org/10.1017/S0022112090001033.
[7] F. Jomni, F. Aitken, A. Denat, Dynamics of microscopic bubbles generated by a corona discharge in insulating liquids : Influence of pressure, J. Electrostat. 47 (1999) 49–59, https://doi.org/10.1016/S0304-3886(99)00022-4.
[8] J. Zahradník, M. Fialová, V. Linek, The effect of surface-active additives on bubble coalescence in aqueous media, Chem. Eng. Sci. 54 (1999) 4757–4766, https://doi.org/10.1016/S0009-2509(99)00192-X.
[9] J. Lee, M. Ashokkumar, S. Kentish, F. Grieser, Determination of the Size of Acoustic Cavitation Bubbles by Pulsed Sonoluminescence, J. Am. Chem. Soc. 127 (2005) 16810–16811. ttp://hdl.handle.net/11343/55433.
[10] D. Sunartio, M. Ashokkumar, F. Grieser, Study of the coalescence of acoustic bubbles as a function of frequency, power, and water-soluble additives, J. Am. Chem. Soc. 129 (2007) 6031–6036, https://doi.org/10.1021/ja068980w.
[11] M. Ashokkumar, R. Hall, P. Mulvaney, F. Grieser, Sonoluminescence from aqueous alcohol and surfactant solutions, J. Phys. Chem. B 101 (1997) 10845–10850, https://doi.org/10.1021/jp972477b.
[12] A. Martínez-Tarifa, S. Arrojo, O. Louisnard, J. González-García, I. Tudela, Correlation between hydroxyl radical production and theoretical pressure distribution in a sonochemical reactor, Phys. Procedia. 3 (2010) 971–979, https://doi.org/10.1016/j.phpro.2010.01.125.
[13] G. Albarrán, E. Mendoza, Ionizing radiation induced degradation of salicylic acid in aqueous solution, Radiat. Phys. Chem. 147 (2018) 27–34, https://doi.org/10.1016/j.radphyschem.2018.01.025.
[14] P. Fernández-Castro, M. Vallejo, M.F. San Román, I. Ortiz, Insight on the fundamentals of advanced oxidation processes: role and review of the determination methods of reactive oxygen species, J. Chem. Technol. Biotechnol. 90 (2015) 796–820, https://doi.org/10.1002/jctb.4634.
[15] L.P. Amin, P.R. Gogate, A.E. Burgess, D.H. Bremner, Optimization of a hydrodynamic cavitation reactor using salicylic acid dosimetry, Chem. Eng. J. 156 (2010) 165–169, https://doi.org/10.1016/j.cej.2009.09.043.
[16] B.S. Karnik, S.H. Davies, M.J. Baumann, S.J. Masten, Use of salicylic acid as a model compound to investigate hydroxyl radical reaction in an ozonation-membrane filtration hybrid process, Environ. Eng. Sci. 24 (2007) 852–860, https://doi.org/10.1089/ees.2006.0156.
[17] E. Peralta, G. Roa, J.A. Hernandez-Servin, R. Romero, P. Balderas, R. Natividad, Hydroxyl radicals quantification by UV spectrophotometry, Electrochim. Acta 129 (2014) 137–141, https://doi.org/10.1016/j.electacta.2014.02.047.
[18] L. Milne, I. Stewart, D.H. Bremner, Comparison of hydroxyl radical formation in aqueous solutions at different ultrasound frequencies and powers using the salicylic acid dosimeter, Ultrason. Sonochem. 20 (2013) 984–989, https://doi.org/10.1016/j.ultsonch.2012.10.020.
[19] S. Arrojo, C. Nerín, Y. Benito, Application of salicylic acid dosimetry to evaluate hydrodynamic cavitation as an advanced oxidation process, Ultrason. Sonochem. 14 (2007) 343–349, https://doi.org/10.1016/j.ultsonch.2006.06.007.
[20] A.G. Chakinala, P.R. Gogate, A.E. Burgess, D.H. Bremner, Intensification of hydroxyl radical production in sonochemical reactors, Ultrason. Sonochem. 14 (2007) 509–514, https://doi.org/10.1016/j.ultsonch.2006.09.001.
[21] A. Martínez-Tarifa, S. Arrojo, A.L. Ávila-Marín, J.A. Pérez-Jiménez, V. Sáez, M.L. Ruiz-Lorenzo, Salicylic acid dosimetry applied for the statistical determination of significant parameters in a sonochemical reactor, Chem. Eng. J. 157 (2010) 420–426, https://doi.org/10.1016/j.cej.2009.11.031.
[22] R. Singla, M. Ashokkumar, F. Grieser, The mechanism of the sonochemical degradation of benzoic acid in aqueous solutions, Res. Chem. Intermed. 30 (2004) 723–733, https://doi.org/10.1163/1568567041856963.
[23] M. Zupanc, T. Kosjek, M. Petkovšek, M. Dular, B. Kompare, B. Širok, Ž. Blažeka, E. Heath, Removal of pharmaceuticals from wastewater by biological processes, hydrodynamic cavitation and UV treatment, Ultrason. Sonochem. 20 (2013) 1104–1112, https://doi.org/10.1016/j.ultsonch.2012.12.003.
[24] G. Albarran, R.H. Schuler, Concerted effects in the reaction of ·OH radicals with aromatics: Radiolytic oxidation of salicylic acid, Radiat. Phys. Chem. 67 (2003) 279–285, https://doi.org/10.1016/S0969-806X(03)00052-5.
[25] M. Zupanc, Ž. Pandur, T. Stepišnik Perdih, D. Stopar, M. Petkovšek, M. Dular, Effects of cavitation on different microorganisms: the current understanding of the mechanisms taking place behind the phenomenon. A review and proposals for further research, Ultrason. Sonochem. 57 (2019) 147–165, https://doi.org/10.1016/j.ultsonch.2019.05.009.
[26] R. Hu, L. Zhang, J. Hu, Study on the kinetics and transformation products of salicylic acid in water via ozonation, Chemosphere 153 (2016) 394–404, https://doi.org/10.1016/j.chemosphere.2016.03.074.
[27] S. Gligorovski, R. Strekowski, S. Barbati, D. Vione, Environmental implications of hydroxyl radicals (•OH), Chem. Rev. 115 (2015) 13051–13092, https://doi.org/10.1021/cr500310b.
[28] M.R. Luo, Encyclopedia of Color Science and Technology, Springer Science + Business Media Singapore 2016, Singapore, 2016. doi: 10.1007/978-3-642-27851-8.
[29] M.U. Rehman, P. Jawaid, H. Uchiyama, T. Kondo, Comparison of free radicals formation induced by cold atmospheric plasma, ultrasound, and ionizing radiation, Arch. Biochem. Biophys. 605 (2016) 19–25, https://doi.org/10.1016/j.abb.2016.04.005.
[30] D.L. Currell, G. Wilheim, S. Nagy, The effect of certain variables on the ultrasonic cleavage of phenol and of pyridine, J. Am. Chem. Soc. 85 (1963) 127–130, https://doi.org/10.1021/ja00885a002.
[31] D. Sunartio, M. Ashokkumar, F. Grieser, The influence of acoustic power on multibubble sonoluminescence in aqueous solution containing organic solutes, J. Phys. Chem. B. 109 (2005) 20044–20050, https://doi.org/10.1021/jp052747n.
[32] J. Lee, K. Yasui, T. Tuziuti, T. Kozuka, A. Towata, Y. Iida, Spatial distribution enhancement of sonoluminescence activity by altering sonication and solution conditions, J. Phys. Chem. B 112 (2008) 15333–15341, https://doi.org/10.1021/jp8060224.
[33] C.L. Henry, C.N. Dalton, L. Scruton, V.S.J. Craig, Ion-specific coalescence of bubbles in mixed electrolyte solutions, J. Phys. Chem. C 111 (2007) 1015–1023, https://doi.org/10.1021/jp066400b.